Critical Doping for the Onset of a Two-Band Superconducting Ground State in $SrTiO_{3-\delta}$

Xiao Lin,[1] German Bridoux,[1] Adrien Gourgout,[1] Gabriel Seyfarth,[2] Steffen Krämer,[2] Marc Nardone,[3] Benoît Fauqué,[1] and Kamran Behnia[1,*]

[1]*Laboratoire de Physique et d'Étude des Matériaux-CNRS (ESPCI and UPMC), Paris 75005, France*
[2]*Laboratoire National des Champs Magnétiques Intenses-CNRS (UJF, UPS and INSA), Grenoble 38042, France*
[3]*Laboratoire National des Champs Magnétiques Intenses-CNRS (UJF, UPS and INSA), Toulouse 31400, France*

(Received 7 January 2014; published 21 May 2014)

In doped $SrTiO_3$ superconductivity persists down to an exceptionally low concentration of mobile electrons. This restricts the relevant energy window and possible pairing scenarios. We present a study of quantum oscillations and superconducting transition temperature T_c as the carrier density is tuned from 10^{17} to 10^{20} cm^{-3} and identify two critical doping levels corresponding to the filling thresholds of the upper bands. At the first critical doping, which separates the single-band and the two-band superconducting regimes in oxygen-deficient samples, the steady increase of T_c with carrier concentration suddenly stops. Near this doping level, the energy dispersion in the lowest band displays a downward deviation from parabolic behavior. The results impose new constraints for microscopic pairing scenarios.

DOI: 10.1103/PhysRevLett.112.207002 PACS numbers: 74.20.Fg, 71.18.+y, 74.25.Dw

Superconductivity is induced in insulating $SrTiO_3$ by introducing n-type charge carriers through chemical doping [1] and survives over 3 orders of magnitude of carrier concentration. The transition temperature T_c peaks to 0.45 K around a carrier density of $n_H \sim 10^{20}$ cm^{-3} [2]. A superconducting dome has also been detected in the metallic interfaces of $SrTiO_3$ [3] when the carrier density is modulated by a gate voltage bias [4]. In unconventional superconductors, such as high-T_c cuprates, superconducting domes are often attributed to the proximity of a magnetic order or a Mott insulator. The recent discovery of a superconducting dome in gate-tuned MoS_2 [5] in the absence of a competing order, however, highlights the limits of our current understanding of the interplay between carrier concentration and superconductivity and motivates a fresh reexamination of superconducting domes. In the specific case of $SrTiO_3$, superconductivity occurs in the vicinity of an aborted ferroelectric order [6] and survives deep inside the dilute metallic regime when the Fermi temperature becomes more than one order of magnitude lower than the Debye temperature [7]. This is a second puzzle in addition to the one raised by the drop in T_c on the overdoped side. These two questions, raised at the opposite limits of the superconducting dome, remain unsettled.

According to band calculations [8–10], doping $SrTiO_3$ with n-type carriers can fill three bands one after the other. Once the critical threshold for the occupation of a band is attained, a new Fermi surface concentric with the previous one emerges. Previous studies of quantum oscillations in bulk doped $SrTiO_3$ [7,11–13] have detected both multiple-frequency [7,12,13] and single-frequency [7,13] oscillations at different doping levels, but did not determine these critical doping levels. Moreover, according to tunneling experiments, doped $SrTiO_3$ beyond a carrier density of 10^{19} cm^{-3} is a multigap superconductor [14]. The interplay between multiband occupation in the normal state and multigap superconductivity has been a subject of recent theoretical attention [21].

We present a systematic study of quantum oscillations and the superconducting transition as a function of carrier concentration n_H extended down to 10^{17} cm^{-3}, 2 orders of magnitude below the range of the tunneling study [14], and find three new results. First of all, the two critical dopings [10] n_{c1} and n_{c2} are identified and the magnitude of the cyclotron mass and the Fermi energy of each band are determined. Second, we find that n_{c1}, the threshold of occupation of the second band, separates two distinct regimes of superconductivity. Below n_{c1}, the superconductor is single band with a large T_c/T_F. Above n_{c1}, it becomes two band with a T_c, that fails to keep the same pace with increasing T_F. Finally, we find that the lowest band presents a deviation from parabolic dispersion near n_{c1}. We conclude that the attractive interaction between electrons, remarkably strong when the chemical potential is near the bottom of this band, significantly weakens when it shifts upward and other bands are occupied. This feature, combined with the low cutoff frequency imposed by the small Fermi energy, drastically limits the choice of the bosonic mode exchanged by Cooper pairs.

Figure 1(a) shows the variation of the frequency of the quantum oscillations with doping in eighteen different samples of n-doped $SrTiO_3$ (see the Supplemental Material [15] for an extensive discussion of the samples). The samples studied were either commercial niobium-doped samples or reduced samples obtained by annealing stoichiometric $SrTiO_3$ in vacuum [7,16]. In most cases, what was measured was the Shubnikov–de Haas (SdH) effect (quantum oscillations of the magnetoresistance). In seven samples,

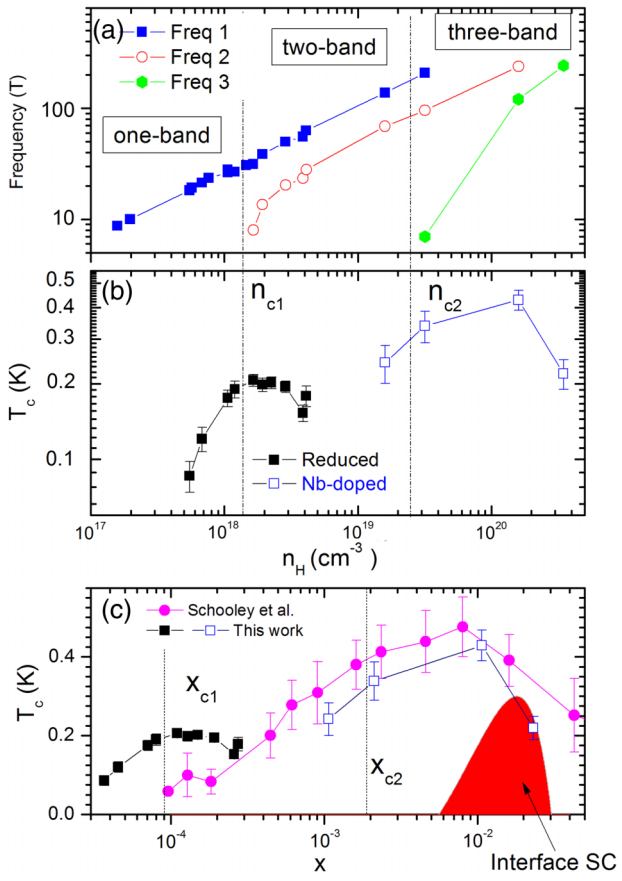

FIG. 1 (color online). (a) Detected frequencies of quantum oscillations as a function of carrier concentration. At two critical doping levels, designated as n_{c1} and n_{c2}, a new frequency emerges. At each critical doping a new band starts to be occupied. (b) Superconducting resistive transition temperature (on a logarithmic axis) as a function of carrier concentration. Solid squares represent reduced samples ($SrTiO_{3-\delta}$) and open squares Nb-doped samples ($SrTi_{1-x}Nb_xO_3$ with $x = 0.02$, 0.01, 0.002, and 0.001). Error bars represent the width of transition. (c) T_c (on a linear axis) as a function of carrier per formula unit. Our data are compared with those reported by Schooley and co-workers [2]. The red shaded region shows the rough contours of superconductivity in the $SrTiO_3/LaAlO_3$ interface [4,17,18].

the Nernst effect was also measured and found to display giant oscillations with a frequency identical to the SdH effect as reported previously [7]. As seen in the figure, the main frequency smoothly evolves with doping. Moreover, at two critical doping levels new frequencies emerge. Figure 1(b) shows the evolution of the superconducting transition temperature of the same samples. The most underdoped samples ($n_H < 4 \times 10^{17}$ cm^{-3}) did not show a superconducting transition down to 60 mK. Nevertheless, they presented a sharp Fermi surface, indicating that superconductivity is preceded by (or concomitant with) the intersection of the chemical potential and the bottom of the conduction band. The most striking feature of the figure is a clear change in the slope of $T_c(n)$ in the vicinity of n_{c1}. This is the first new result of this study.

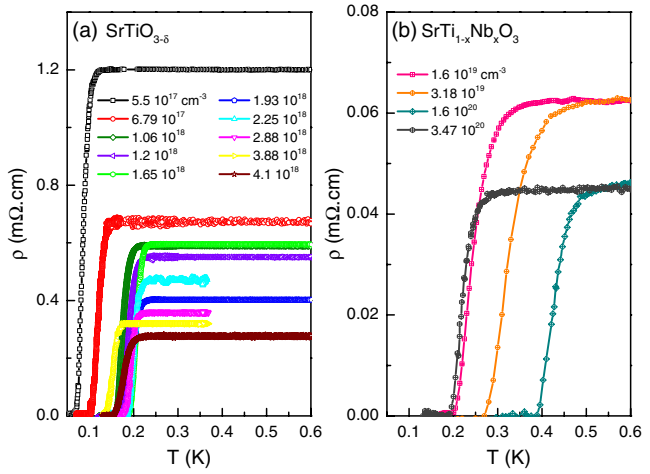

FIG. 2 (color online). Low-temperature resistivity of reduced (a) and Nb-doped (b) single crystals. Note the continuous evolution of resistive transitions in reduced samples. As the doping increases, the transition first shifts to higher temperatures and then remains more or less constant.

Figure 1(c) compares our data with the early work reported by Schooley *et al.* [2]. For each sample, the error bar represents the width of the resistive transition, i.e., the interval between two temperatures corresponding to 0.1 and 0.9 drops in resistivity (see our data in Fig. 2). While the two sets of data match roughly with each other, the structure in the dilute limit is far more clear in our data. The panel shows also the interface dome, restricted to a narrow window far above the concentration range scrutinized by this work. The evolution of resistive superconducting transitions with carrier concentration across n_{c1} is visible in Fig. 2.

The SdH data leading to an unambiguous identification of n_{c1} are presented in Fig. 3. The oscillating component of magnetoresistance, obtained after the subtraction of a smooth background (obtained by a polynomial fit), is plotted as a function of the inverse of magnetic field times the main frequency. The sample with the lowest carrier concentration shows a single set of oscillations with split peaks. We attribute this splitting to the presence of tetragonal domains in our crystals. Recently, Allen *et al.* [13], by performing an angle-dependent Shubnikov–de Haas study, found that the Fermi surface of the lower band is larger along k_z than along either k_x or k_y. In our study, the magnetic field is applied along the cubic [100] axis. Below 105 K, in the tetragonal phase, our samples can host three domains corresponding to the three possible orientations for the tetragonal z axis. As illustrated in Fig. 3(b), there would be two possible magnitudes for the cross section of the Fermi surface, when the magnetic field is along the nominal [100] axis. In this case, the main frequency corresponds to the smaller cross section, which is 2 times more likely to occur than the larger one. As discussed in detail in the Supplemental Material [15], this interpretation is in very good agreement with the known topology of the Fermi surface.

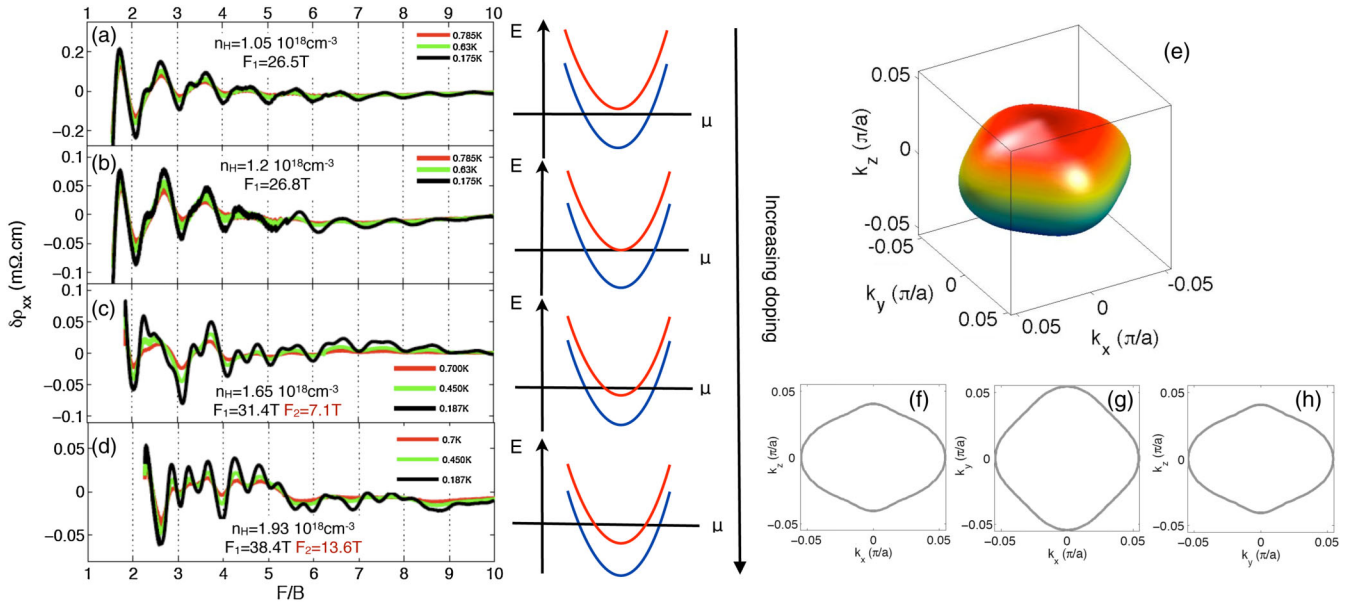

FIG. 3 (color online). Left: a new frequency emerges in the Shubnikov–de Haas data in the vicinity of n_{c1}. When the carrier density is below n_{c1}, quantum oscillations display a single periodicity with split peaks and each peak is more prominent than its preceding neighbor (a). With increasing carrier density, a second frequency emerges on top of the first one (b)–(d). Data are plotted as a function of the inverse of magnetic field normalized by the principal frequency F_1 in order to simplify comparison. The Fermi surface of the lower band according to Ref. [13] is shown in panel (e) and its projection along the three high-symmetry axes in panels (f) and (g). In multidomain crystals, the two possible Fermi cross sections give rise to split peaks in quantum oscillations.

As seen in panels (a)–(d) of Fig. 3, at the concentration of 1.2×10^{18} cm^{-3} beating emerges and indicates the presence of a second set of oscillations with a significantly longer period. In samples with $n_H > n_{c1} = 1.2 \times 10^{18}$ cm^{-3}, the presence of this second frequency becomes clear and then it rapidly grows with increasing doping. The frequencies were quantified both by a FFT analysis of our data (see the Supplemental Material [15]) and direct identification of the two periods in the data.

Analysis of quantum oscillations using the Lifshitz-Kosevitch formalism yields the magnitude of the cyclotron mass. The results of the analysis are shown in the upper panel of Fig. 4. We find that below n_{c1}, the effective cyclotron mass in the lower band, m_1, keeps a steady magnitude of $1.5 - 1.8m_e$, as previously reported [7]. At higher doping levels, m_1 becomes as large as $4m_e$. In this doping range, the middle band hosts significantly lighter carriers ($m_2 \sim 1.3m_e$).

Comparing the total density of carriers distributed in the three bands and the carrier concentration obtained by measuring the Hall number, one can check the consistency of the emerging overall picture. Assuming three spherical Fermi surfaces leads to Fig. 4(b). As seen in the figure, up to n_{c2} the two concentrations remain close to each other. The ratio of the two remains lower than unity, which is an expected consequence of the contrast between the assumed sphericity of the Fermi surface and its moderate anisotropy according to both experiment [12,13] and theory [8,10]. As discussed in the Supplemental Material [15], the measured anisotropy of the Fermi surface below n_{c1} [13] gives a satisfactory account of n_{SdH}/n_H in our data. At the carrier density of 1.6×10^{20} cm^{-3}, three bands are filled, but experiment detects only two frequencies [see Fig. 1(a)]. It is straightforward to identify both the missing band and the reason of its absence. Only in the two upper bands is the mobility high enough for detectable quantum oscillations in a magnetic field of 17 T. The total density of carriers concentrated in these two visible bands is well below the total carrier concentration [see Fig. 4(b)]. Both of these features point to the lower band (which contains most of the carriers, but those with less mobility) as the one that becomes invisible at this doping level.

Now, we can address a central issue in the description of the band structure in this system. According to the picture first sketched by Mattheiss [8], the t_{2g} orbitals of titanium atoms give rise to a threefold degenerate band [9,10]. The degeneracy is lifted by a combination of spin-orbit coupling and tetragonal distortion. Recently, van der Marel and co-workers [10] pointed out that the energy gap between the bands and the peculiarity of their dispersion crucially depends on the choice of parameters. Our experiment finds that the effective mass in the lower band begins to increase as soon as the average radius of the Fermi surface exceeds 3×10^8 m^{-1}. As illustrated in Figs. 4(d) and 4(e), this feature is in good agreement with the choice of parameters in Ref. [10], which leads to a nonparabolic dispersion for the lower band in the absence of interaction. On the other hand the amplitude of the cyclotron mass and the size of

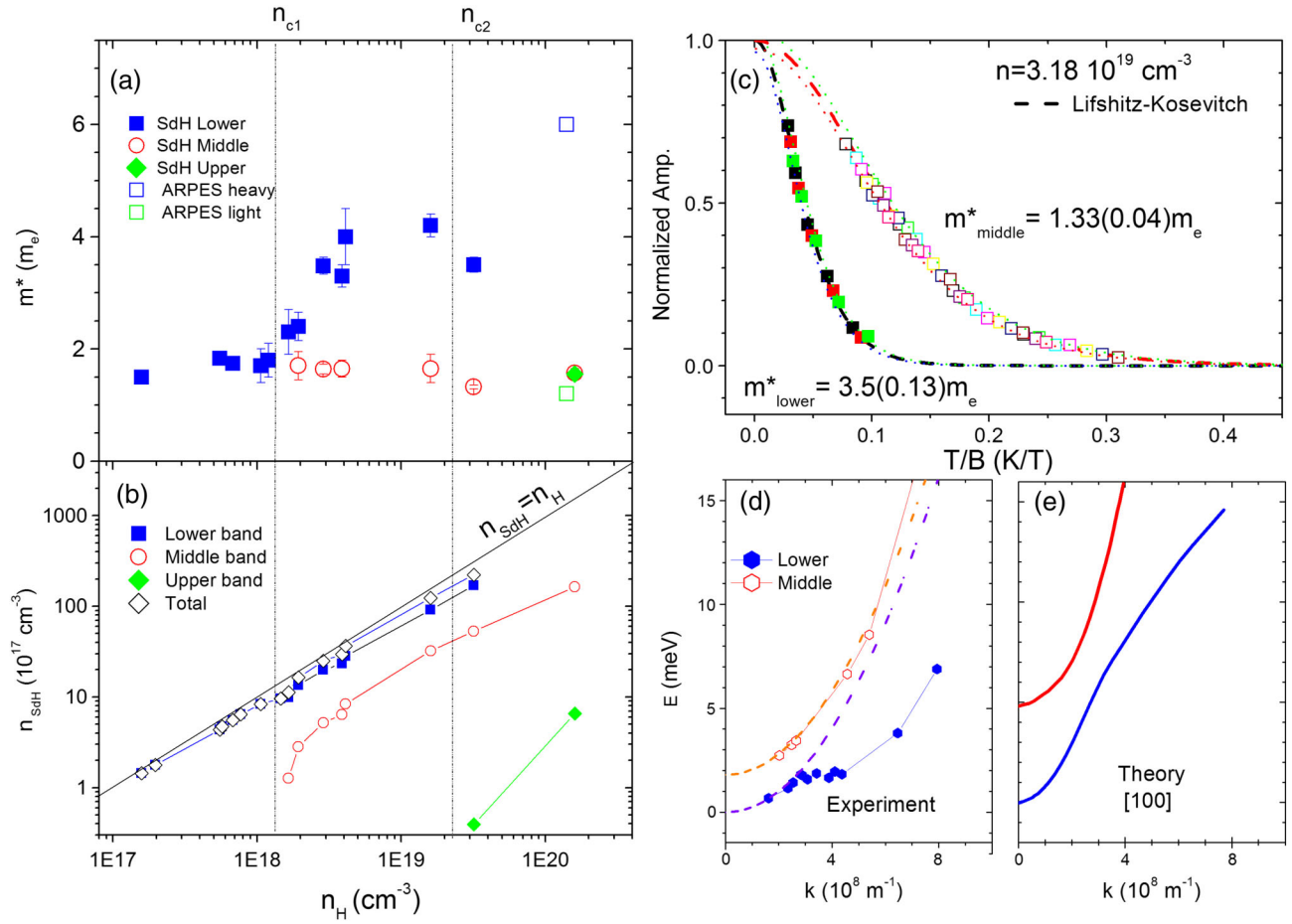

FIG. 4 (color online). (a) The effective mass in each band as a function of carrier concentration. The masses reported by an angle resolved photoemission spectroscopy study on a bulk sample at $n = 1.4 \times 10^{20}$ cm^{-3} [19] is also shown for comparison. (b) Carrier concentration and its distribution among bands according to the detected frequency and assuming spherical Fermi surfaces. The total carrier density falls just below the Hall carrier density. Above 1.6×10^{20} cm^{-3}, the lower band becomes invisible because of its reduced mobility. (c) Lifshitz-Kosevitch analysis of the oscillations revealing two distinct masses for the lower and middle bands. Each color corresponds to a different oscillation. (d) The Fermi energy, defined as $\hbar^2 k_F^2/2m_c$ in the two lower bands plotted as a function of corresponding k_F. The middle band is shifted upward by the energy gap between the two bands. (e) Theoretical energy dispersion near the bottom of the bands according to Ref. [10].

the gaps differs significantly between noninteracting theory and experiment. The experimentally determined mass at the bottom of the band ($1.5m_e$) is twice as large as the theoretical expectation [10]. As a consequence of mass renormalization, commonly attributed to electron-phonon interaction [20], the gap between the lower and middle bands (the Fermi energy of the lower band at $n = n_{c1}$) is 1.8 meV, significantly lower than the expected value of 4.3 meV in the noninteracting band picture [10].

The main outcome of this study is to identify a critical doping n_{c1}, below which a single band is occupied and T_c rapidly rises with doping. In this regime, the T_c/T_F ratio is as large as 0.01, comparable to many unconventional superconductors [7]. This process is interrupted when the carrier concentration exceeds n_{c1}. This highlights the specificity of multiband superconductivity in $SrTiO_3$, the subject of a recent theoretical work [21]. Motivated by the experimental reports on the variation of T_c near n_{c2} [14], Fernandes and co-workers considered the variation of the superconducting transition temperature across a critical doping for different combinations of positive interband (λ_{ij}) and intraband (λ_{ii}) superconducting coupling parameters and found that filling an upper band (labeled 2) in addition to a lower band (labeled 1) would enhance T_c. The larger the ratios of $\lambda_{12}/\lambda_{11}$ and/or $\lambda_{22}/\lambda_{11}$, the more drastic is the expected enhancement. This contrasts with our experimental observation of a drop in $T_c(n)$ near n_{c1}.

This discrepancy calls for a theoretical reexamination extended to negative (i.e., repulsive) λ_{22} and λ_{12}. More importantly, in this analysis, λ_{ii} has been taken to be a constant V_i (representing overall attractive interaction between electrons) times $N_i(0)$, the density of states at the Fermi energy at band i. This assumption can only generate a monotonically increasing critical temperature,

since the density of states unavoidably increases with carrier concentration. The existence of domes implies that this approximation does not hold and points to a nontrivial evolution of V_1 as the outer Fermi surface expands.

Below n_{c1}, the normal state of superconducting $SrTiO_3$ is a metal with a Fermi energy as low as 1 meV and thus the bosons exchanged between pairing electrons cannot be typical phonons with a Debye energy more than one order of magnitude larger [7]. One candidate to replace them at small wave vectors is a plasmonic mode suggested by Takada [22]. Another one, invoked by Appel [23], is the soft mode observed below the 105 K structural transition [24]. Our results frame the challenge faced by such propositions in a multigap context. The attractive interaction should couple electronic states more efficiently below n_{c1}, i.e., when the Fermi surface is single component and the dispersion is still parabolic.

In spite of its notorious inability to predict new superconductors [25], the BCS theory has been successfully employed to give an account of unexpectedly discovered superconductors such as MgB_2 [26]. In the case of $SrTiO_3$, the challenge to theory is framed with exceptional sharpness and few *ad hoc* parameters. The combination of a simple Fermi surface topology, a very narrow energy window, and a wide superconducting dome with fine details provides an exceptional opportunity to test the expected link between the critical temperature, the electronic density of states, and the effective electron-electron interaction.

We thank A. Balatsky, R. Fernandes, D. van der Marel, I. Mazin, and J.-M. Triscone for discussions. This work is supported by Agence Nationale de la Recherche as part of QUANTHERM and SUPERFIELD projects and by EuroMagNET II under EU Contract No. 228043. K. B. acknowledges the hospitality of the Aspen Physics Center.

*kamran.behnia@espci.fr

[1] J. F. Schooley, W. R. Hosler, and M. L. Cohen, Phys. Rev. Lett. **12**, 474 (1964).
[2] J. F. Schooley, W. R. Hosler, E. Ambler, J. H. Becker, M. L. Cohen, and C. S. Koonce, Phys. Rev. Lett. **14**, 305 (1965).
[3] A. Ohtomo and H. Y. Hwang, Nature (London) **427**, 423 (2004).
[4] A. D. Caviglia, S. Gariglio, N. Reyren, D. Jaccard, T. Schneider, M. Gabay, S. Thiel, G. Hammerl, J. Mannhart, and J.-M. Triscone, Nature (London) **456**, 624 (2008).
[5] J. T. Ye, Y. J. Zhang, R. Akashi, M. S. Bahramy, R. Arita, and Y. Iwasa, Science **338** 1193 (2012).
[6] K. A. Müller and H. Burkard, Phys. Rev. B **19**, 3593 (1979).
[7] X. Lin, Z. Zhu, B. Fauqué, and K. Behnia, Phys. Rev. X **3**, 021002 (2013).
[8] L. F. Mattheiss, Phys. Rev. B **6**, 4718 (1972).
[9] R. Bistritzer, G. Khalsa, and A. H. MacDonald, Phys. Rev. B **83**, 115114 (2011).
[10] D. van der Marel, J. L. M. van Mechelen, and I. I. Mazin, Phys. Rev. B **84**, 205111 (2011).
[11] B. Gregory, J. Arthur, and G. Seidel, Phys. Rev. B **19**, 1039 (1979).
[12] H. Uwe, R. Yoshizaki, T. Sakudo, A. Izumi, and T. Uzumaki, Jpn. J. Appl. Phys. **24**, 335 (1985).
[13] S. J. Allen, B. Jalan, S. B. Lee, D. G. Ouellette, G. Khalsa, J. Jaroszynski, S. Stemmer, and A. H. MacDonald, Phys. Rev. B **88**, 045114 (2013).
[14] G. Binnig, A. Baratoff, H. E. Hoenig, and J. G. Bednorz, Phys. Rev. Lett. **45**, 1352 (1980).
[15] See Supplemental Material at http://link.aps.org/supplemental/10.1103/PhysRevLett.112.207002 for detailed list of samples and subtleties of Fermi surface anisotropy.
[16] A. Spinelli, M. A. Torija, C. Liu, C. Jan, and C. Leighton, Phys. Rev. B **81**, 155110 (2010).
[17] C. Bell, S. Harashima, Y. Kozuka, M. Kim, B. G. Kim, Y. Hikita, and H. Y. Hwang, Phys. Rev. Lett. **103**, 226802 (2009).
[18] C. Richter *et al.*, Nature (London) **502**, 528 (2013).
[19] Y. J. Chang, A. Bostwick, Y. S. Kim, K. Horn, and E. Rotenberg, Phys. Rev. B **81**, 235109 (2010).
[20] J. L. M. van Mechelen, D. van der Marel, C. Grimaldi, A. B. Kuzmenko, N. P. Armitage, N. Reyren, H. Hagemann, and I. I. Mazin, Phys. Rev. Lett. **100**, 226403 (2008).
[21] R. M. Fernandes, J. T. Haraldsen, P. Wölfle, and A. V. Balatsky, Phys. Rev. B **87**, 014510 (2013).
[22] Y. Takada, J. Phys. Soc. Jpn. **49** 1267 (1980).
[23] J. Appel, Phys. Rev. **180**, 508 (1969).
[24] G. Shirane, Rev. Mod. Phys. **46**, 437 (1974).
[25] J. E. Hirsch, Phys. Scr. **80**, 035702 (2009).
[26] H. J. Choi, D. Roundy, H. Sun, M. L. Cohen, and S. G. Louie, Nature (London) **418**, 758 (2002).